ROYAL SOCIETY
OF CHEMISTRY

PAPER

Check for updates

Can COFs replace MOFs in flue gas separation? high-throughput computational screening of COFs for CO_2/N_2 separation†

Omer Faruk Altundal, Cigdem Altintas [ID] and Seda Keskin [ID] *

Covalent organic frameworks (COFs) are under study as adsorbent and membrane candidates for gas separation applications. However, experimental testing of all synthesized COF materials as adsorbents and membranes under different operating conditions is not practical. Herein, we used a high-throughput computational screening approach to investigate adsorption- and membrane-based flue gas separation performances of 295 COFs. Adsorption selectivity, working capacity, percent regenerability and adsorbent performance score of COFs were calculated for separation of CO_2/N_2 mixture for three different cyclic adsorption processes, pressure swing adsorption (PSA), vacuum swing adsorption (VSA) and temperature swing adsorption (TSA). The top performing COFs were identified for each process based on the combination of several metrics. Selectivities of the top COFs were predicted to be greater than those of zeolites and activated carbons. Molecular simulations were performed considering the wet flue gas for the top COF adsorbents and results revealed that most COFs retained their high CO_2 selectivities in the presence of water. Using COFs with detailed geometry optimization and high-accuracy partial charges in molecular simulations led to lower selectivities and adsorbent performance scores compared to using experimentally reported COFs with approximate charges. Membrane-based flue gas separation performances of COFs were also studied and most COFs were found to have comparable CO_2 permeabilities with metal organic frameworks (MOFs), up to 3.96×10^6 barrer, however their membrane selectivities were lower than MOFs, 0.38–21, due to their large pores and the lack of metal sites in their frameworks. Structure–performance relations revealed that among the COFs we studied, the ones with pore sizes <10 Å, accessible surface areas <4500 m^2 g^{-1} and 0.6 < porosity <0.8 are not only highly selective adsorbents but also CO_2 selective membranes.

1. Introduction

Carbon dioxide (CO_2) capture from flue gas, CO_2/N_2 mixture, is environmentally, industrially, and economically important.[1,2] Adsorption-based gas separation techniques such as pressure swing adsorption (PSA), vacuum swing adsorption (VSA), and temperature swing adsorption (TSA) have been used for flue gas separation.[3,4] An ideal adsorbent should simultaneously offer high selectivity and high working capacity[5,6] in addition to being

Department of Chemical and Biological Engineering, Koc University, Rumelifeneri Yolu, Sariyer, 34450, Istanbul, Turkey. E-mail: skeskin@ku.edu.tr; Tel: +90-212-338-1362

† Electronic supplementary information (ESI) available: Comparison of CO_2 uptakes obtained from GCMC simulations with experimental results; distribution of atoms for screened COFs; comparison of $R\%$ and N_{des} values for TSA and VSA conditions; comparison of CO_2 uptakes of CURATED and CoRE COFs obtained from GCMC simulations for CO_2/N_2 : 15/85 mixture at VSA, PSA, and TSA conditions; comparison of calculated S_{ads} and ΔN values of CURATED and CoRE COFs for VSA, PSA, and TSA conditions according to their ASA ratios; comparison of calculated APSs of CURATED and CoRE COFs according to their density and porosity ratios. See DOI: 10.1039/d0ta04574h

robust under cyclic operation conditions. Activated carbons and zeolites have been utilized as adsorbents but they have limited selectivity and regenerability.[7] Therefore, identification of new adsorbent materials offering the best combination of CO_2 capacity, CO_2/N_2 selectivity and regenerability has been a long-standing goal.

Metal organic frameworks (MOFs) are porous structures in which nodes consisting of metal clusters are connected through organic linkers.[8] The large variety of metal ions and organic linkers enabled the synthesis of many different materials with tunable chemistries, low densities (0.2 g cm^{-3}), large surface areas (>6000 m^2 g^{-1}), various pore sizes and high porosities (0.3–0.9).[9,10] MOFs have been considered as promising materials for adsorption-based CO_2/N_2 separation due to these structural and chemical aspects.[11,12] Several computational studies used Grand Canonical Monte Carlo (GCMC) simulations to predict CO_2/N_2 separation performances of various MOFs.[13,14] For example, early studies showed CuBTC had a slightly higher CO_2/N_2 selectivity (~33) than zeolite MFI (~27) for separation of CO_2/N_2 : 15/85 mixture at PSA condition.[13] Krishna and van Baten[15] showed that MgMOF-74 has a similar selectivity to that

This journal is © The Royal Society of Chemistry 2020

J. Mater. Chem. A, 2020, **8**, 14609–14623 | **14609**

of NaX ($\sim$200) with a higher working capacity ($\sim$3 mol kg^{-1}) than that of NaX ($\sim$2 mol kg^{-1}) for CO_2/N_2 : 15/85 mixture at VSA condition at 300 K. With these, the promise of MOFs in adsorption-based CO_2/N_2 separation has been proven.[16–18]

Due to the acceleration in the synthesis of MOFs, experimental investigation of MOFs for flue gas separation has become challenging. High-throughput computational screening methods have been very useful for efficiently screening large numbers of MOFs to guide experimental studies to more promising MOFs. The first high-throughput screening of MOFs for CO_2/N_2 separation was carried out by studying 489 MOFs and two MOFs were highlighted with their high CO_2/N_2 mixture selectivities (269 and 197) at 1 bar, 303 K.[19] Wu et al.[20] studied 105 different MOFs and showed that higher CO_2/N_2 selectivities (>120) can be obtained at 1 bar, 298 K if the isosteric heats of adsorption of CO_2 and N_2 is highly different in MOFs having low porosities. Wilmer et al.[21] examined flue gas separation potentials of 130 000 hypothetical MOFs at VSA condition at 298 K and showed that the best materials have pore sizes <5 Å, porosities in the range of 0.3–0.4. Qiao et al.[22] screened 4764 MOFs[23] for flue gas separation at VSA condition and showed that most of the promising MOFs have lanthanides. Our group recently computed several adsorbent performance evaluation metrics of 3816 MOFs for separation of CO_2/N_2 mixture at VSA conditions and reported that the best MOF candidates have 3.8 Å < pore limiting diameter <5 Å and surface area <1000 m^2 g^{-1}.[10] Molecular simulations were also used to investigate membrane-based flue gas separation potential of MOFs. For example, Krishna and van Baten[24] screened a large number of MOF, zeolitic imidazolate framework (ZIF), and zeolite membranes using Configurational-Bias Monte Carlo (CBMC) and Molecular Dynamics (MD) simulations. They reported that CO_2/N_2 selectivity ($\sim$20) and CO_2 permeability ($\sim$8 × 10^5 barrer) of Mg-MOF-74 was higher than those of many zeolites (DDR, ERI, MFI, TSC, and FAU). Watanabe and Sholl[25] calculated CO_2 permeabilities and CO_2/N_2 selectivities of 179 MOFs at infinite dilution and reported that MOF membranes offer superior CO_2 permeabilities (10^4 barrer) and CO_2/N_2 selectivities (>100) than polymeric membranes. Our group recently studied 3806 MOF membranes at infinite dilution and the top 15 MOFs having high CO_2/N_2 selectivity in the range of 16–820 at 1 bar, 298 K were identified.[26] All these works revealed the high potential of MOF adsorbents and membranes for CO_2/N_2 separation. However, MOFs offering the highest CO_2 separation performances under dry flue gas condition may suffer from a decrease in CO_2 selectivity and/or a stability issue under humid environment and therefore, the search for robust MOFs and MOF-like materials is still continuing.[27–32]

Covalent organic frameworks (COFs) are a class of porous materials containing light elements (hydrogen, boron, carbon, nitrogen, oxygen, silicon) linked by strong covalent bonds, like in diamond.[30,33–37] Since COFs are light materials and have strong covalent bonds, they show low density, good thermal and chemical stability, and permanent porosity.[37] Compared to MOFs, 3-dimensional COFs can offer a higher fraction of accessible surface area for gas adsorption.[38] Tong et al.[39] computationally studied 46 COFs for separation of CH_4/H_2,

CO_2/CH_4, and CO_2/H_2 mixtures at PSA condition and showed that COFs offer better CO_2 working capacities (>3 mol kg^{-1}) than many conventional zeolites and common MOFs. A computation-ready experimental COF database (CoRE COF) consisting of 187 solvent-free COFs was created,[40] later expanded[41] and finally reported to include 309 COFs which facilitated high-throughput computational screening of these materials.[42] Using this database, 290 functionalized COFs were designed and 137 of these COFs were predicted to perform better than conventional polymers for membrane-based CO_2/CH_4 separation.[42] Ongari et al.[43] recently reported a publicly available clean, uniform and refined with automatic tracking from experimental COF database (CURATED COFs) consisting of 324 optimized COFs with high-quality partial charges. Smit's group[44] predicted CO_2 parasitic energy of the CURATED COFs[43] and hypothetical COFs using molecular simulations and showed that many COFs have lower energy than that of tradi-tional amine scrubbing process. As can be seen from this literature summary, we have limited information on the adsorption and membrane-based CO_2/N_2 separation performances of COFs and the high-throughput computational screening of COFs is essential to compare their adsorbent and membrane performance evaluation metrics with those of MOFs.

Motivated from this, in this work, we searched the answer to the following question: can COFs replace or at least compete with MOFs as adsorbent and membrane materials in flue gas separation processes? We first performed a high-throughput computational screening study on CoRE COF database to unlock both adsorption-based and membrane-based CO_2/N_2 separation potentials of all experimentally synthesized COFs. CO_2/N_2 mixture adsorption in COFs was computed using GCMC simulations and results were used to evaluate selectivity, working capacity, adsorbent performance score and regenerability of COF adsorbents at three different cyclic adsorption conditions, PSA, VSA, and TSA. Efficiencies of these three processes were then compared using adsorbent performance evaluation metrics to select the most promising COFs for each operating condition. The effect of humidity on the flue gas separation performance of the most promising COF adsorbents was also investigated by performing simulations for adsorption-based $CO_2/N_2/H_2O$ mixture separation. We also utilized CURATED COF database for molecular simulations and compared the results with those of CoRE COF database to understand how structural curations on the experimentally re-ported COFs affect their predicted CO_2/N_2 separation perfor-mances. We finally assessed membrane-based CO_2/N_2 mixture separation performances of COFs by combining the results of GCMC and MD simulations and compared gas permeabilities and selectivities of COF membranes with those of polymers. The large-scale screening of COFs performed in this work allowed us to elucidate the structure–performance relations that can help to describe the structural features leading to high-performance COF adsorbents and membranes. All these results will (i) provide the first comparison for the flue gas separation performances of COFs, MOFs, and established adsorbents and membranes including zeolites and polymers, (ii) guide the future studies to the most promising COFs identified from high-

14610 | *J. Mater. Chem. A*, 2020, **8**, 14609–14623

This journal is © The Royal Society of Chemistry 2020

throughput screening and (iii) contribute to the intuition at the molecular scale for the design and advancement of new COF adsorbents and membranes with more efficient CO_2 separation potentials.

2. Computational details

2.1. COF database

We used the most recent CoRE COF database in the literature consisting of 309 COF structures.[42] Structural properties of COFs; pore limiting diameter (PLD), largest cavity diameter (LCD), porosity (ϕ), density (ρ) and accessible surface area (ASA) were computed employing Zeo++ software.[45] A probe diameter of 3.72 Å which corresponds to the kinetic diameter of N_2 molecule was used for surface area determination whereas a probe with zero diameter was used for the pore volume calculations. CoRE COF database was then refined to only include the structures with non-null ASA so that both gases can adsorb in the pores. Consequently, 295 COFs remained in the database offering a diverse range of structural properties. Porosities of these COFs were computed to be between 0.44–0.96 while their PLDs and ASAs were calculated to be in the range of 4.19–44.50 Å and 245–8561 m^2 g^{-1}, respectively. We note that atomistic coordinates of HAT-NTBA-COF was corrected by using the coordinates taken from its experimental synthesis paper[46] following the warning in the literature.[43] To examine the effect of structural curations performed on the experimental CoRE COF database, we also studied 23 materials from the CURATED COF database.

2.2. Molecular simulations

We used the high-throughput computational screening approach that we introduced and used for MOFs in our previous works[10,47] where we showed that the results of our molecular simulations were in accordance with experimental CO_2 and N_2 uptakes of MOFs. To compute the CO_2/N_2 mixture adsorption data of COFs, GCMC simulations were performed with RASPA 2.35 simulation code.[48] We specified the composition of CO_2/N_2 as 15/85 to represent dry flue gas. GCMC simulations were performed at three different operating conditions; VSA, PSA, and TSA. For VSA and PSA processes, temperature was fixed at 298 K while adsorption (desorption) pressure was set as 1 (0.1) bar at VSA and 10 (1) bar at PSA. For TSA process, pressure was set as 1 bar and temperatures for adsorption and desorption were set as 298 K and 393 K, respectively.[49] Peng–Robinson equation of state was used for pressure to fugacity conversion. Non-bonded interactions were defined with Lennard-Jones (LJ) potential and a cut-off distance of 14 Å was specified for truncation of these interactions. The number of unit cells in the simulation box was adjusted according to the cut-off distance. Electrostatic interactions between adsorbate–adsorbate and adsorbate-COF atoms were considered due to the quadrupolar moments of CO_2 and N_2. Partial atomic charges of COF atoms were assigned *via* the charge equilibration method (Q_{eq}).[50] The partial charges of atoms in a COF, COF-SDU1, did not converge using the Q_{eq} in the RASPA and assigned by the Q_{eq}

implemented in Materials Studio.[51] The Ewald summation was implemented to incorporate long–range interactions.[52] 10 000 cycles were set for initialization and 20 000 cycles were set for taking ensemble averages in GCMC simulations. Potential parameters for CO_2 molecule were taken from the TraPPE[53] force field. For CO_2 molecule, a three-site rigid model with LJ 12–6 potential was used where the partial point charges were set at the center of each site.[54] Similarly, for N_2 molecule, a three-site model was used with partial charges at the center of mass.[55] DREIDING[56] was used for the potential parameters of COF atoms since this force field was shown to give a good agreement with the experimentally reported single-component CO_2 and CH_4 adsorption isotherms of COFs in the literature.[42] We also showed the good agreement between our simulations using DREIDING and experimentally measured CO_2 adsorption isotherms of several COFs in Fig. S1 of the ESI.† To understand the effect of humidity, $CO_2/N_2/H_2O$: 15/82/3 ternary mixture simulations were performed. The partial pressure of H_2O was kept at 3 kPa, which is 70% of the vapor pressure of H_2O in TIP4P[57,58] model at 298 K (4.3 kPa). The Henry's constants of H_2O in COFs were also calculated to quantify the affinity of COFs to water at 298 K by conducting simulations with only Widom particle insertion move in RASPA using 10^5 cycles.[59] Using the results of GCMC simulations, adsorption selectivity, working capacity, adsorbent performance score and percent regenerability were computed as shown in Table 1 to assess the performances of COF adsorbents for gas separation. CO_2 and N_2 self-diffusivities were calculated using MD simulations which were performed for 5×10^6 cycles in the NVT ensemble with a time step of 1 fs. 10^6 cycles were set both for equilibration and initialization of NVT-MD simulations in which the Nosé–Hoover[60] thermostat was utilized. Self-diffusivities of gases were calculated from the slope of their mean square displacements according to the Einstein's relation.[61] Gas permeabilities and selectivities of COF membranes were predicted by combining the results of GCMC and MD simulations as shown in Table 1. Two feed pressures, 1 bar and 10 bar, were used while the permeate pressure was set as vacuum. Gas loadings obtained from GCMC simulations at 1 bar and 10 bar were used as the input of MD simulations.[62] Atomic coordinates of COF atoms were fixed during calculations to save computational time. Since pore sizes of COFs studied in this work are large enough with respect to the kinetic diameters of both gases, flexibility was expected to not considerably effect our results as we discussed before.[63]

3. Result and discussion

3.1 Adsorption-based separation performances of COFs

We first examined adsorption-based CO_2/N_2 separation potentials of 295 COFs. Fig. 1 represents CO_2/N_2 selectivity of COFs as a function of their CO_2 working capacity at (a) VSA (b) PSA and (c) TSA conditions. CO_2/N_2 selectivity and CO_2 working capacity of 3808 MOFs which were previously computed at VSA condition[10] were also shown in Fig. 1(a). CO_2 selectivities were computed to be between 1–105 and 2–6107 for COFs and MOFs, respectively, whereas CO_2 working capacities were calculated to

This journal is © The Royal Society of Chemistry 2020

J. Mater. Chem. A, 2020, **8**, 14609–14623 | **14611**

Table 1 Calculation of metrics used to evaluate separation performances of COF adsorbents and membranes[a]

Metrics	Formula
Adsorption selectivity	$S_{\text{ads},CO_2/N_2} = \dfrac{N_{CO_2}}{N_{N_2}} \times \dfrac{y_{N_2}}{y_{CO_2}}$
Working capacity (mol kg^{-1})	$\Delta N = N_{\text{ads},CO_2} - N_{\text{des},CO_2}$
Adsorbent performance score (mol kg^{-1})	$\text{APS} = S_{\text{ads},CO_2/N_2} \times \Delta N_{CO_2}$
Percent regenerability	$R\% = \dfrac{\Delta N_{CO_2}}{N_{\text{ads},CO_2}} \times 100\%$
Diffusion selectivity	$S_{\text{diff},CO_2/N_2} = \dfrac{D_{\text{self},CO_2}}{D_{\text{self},N_2}}$
Membrane selectivity	$S_{\text{mem},CO_2/N_2} = S_{\text{ads},CO_2/N_2} \times S_{\text{diff},CO_2/N_2}$
Permeability (barrer)	$P_i = \dfrac{c_{i,\text{ads}} \times D_{\text{self},i}}{f_i}$

[a] i: gas species, CO_2 or N_2. N_{ads} (mol kg^{-1}): gas uptake at adsorption conditions. N_{des} (mol kg^{-1}): gas uptake at desorption conditions. y: composition of the gas species in the bulk phase. f (Pa): partial pressure of gas species in the mixture. c (mol m^{-3}): gas concentration obtained from GCMC simulations. D (m^2 s^{-1}): self-diffusivity of gas obtained from MD simulations. 1 barrer = 3.348×10^{-16} mol $\times$ m (m$^2 \times$ s $\times$ Pa)$^{-1}$.

be between 0.02–1.69 mol kg^{-1} and 0.01–4.16 mol kg^{-1} for COFs and MOFs, respectively. This comparison shows that COFs have lower CO_2/N_2 selectivities than most of the MOFs at VSA condition which can be explained with larger pore sizes of COFs compared to MOFs and the absence of metal sites in COFs. Only 5% of MOFs shown in Fig. 1(a) have LCDs > 15 Å while 70% of

COFs have LCDs > 15 Å. Large pores of COFs allow both gas molecules to be adsorbed in the framework, reducing the selective adsorption property of materials. In addition to this, MOFs have metal sites leading to strong coulombic interactions between the framework atoms and CO_2 molecules.[64] Most COFs do not have those metal sites. For example, in the whole set of
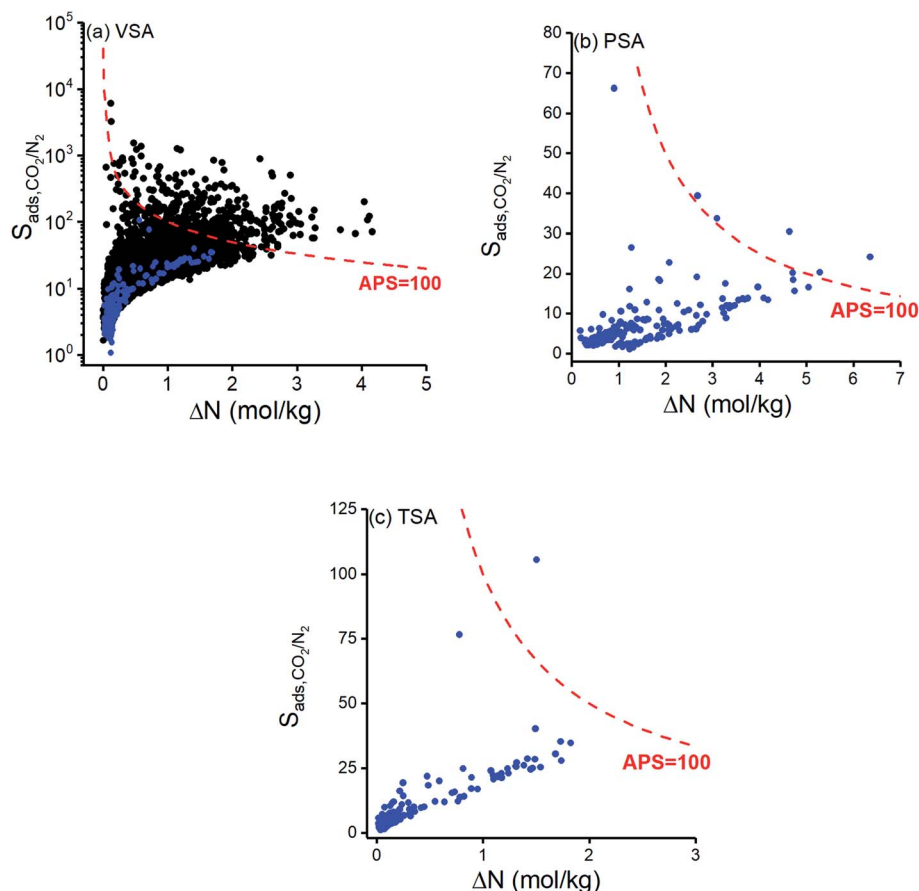

Fig. 1 Predicted selectivity and working capacity of COFs for separation of CO_2/N_2 : 15/85 mixture computed at (a) VSA, (b) PSA, (c) TSA conditions. Separation performances of MOFs (black dots) are also shown in (a) for comparison.

295 COFs that we examined, only 24 COFs have metal sites with relatively high partial charges (8 with Cu sites, 6 with Ni sites, 5 with Zn sites, 4 with Co sites and 1 with Li sites). As a result of this, most COFs have weaker interactions with the adsorbate molecules compared to MOFs. Detailed information about the distribution of elements in COFs that we examined in this work can be seen in Fig. S2.† Performances of the adsorbents are generally assessed by considering both selectivity and working capacity because a promising adsorbent should offer both high working capacity and high selectivity for an efficient and economic gas separation process. We used the adsorbent performance score (APS), which is the multiplication of adsorption selectivity and working capacity as shown in Table 1, to appraise the performances of COFs for CO_2/N_2 separation. We arbitrarily set APS to 100 mol kg^{-1}, as shown with the red curves in Fig. 1, to identify good performing materials. Fig. 1(a) shows that COFs have relatively lower APSs than MOFs mainly due to their lower selectivities at VSA condition. Even the COF with the highest APS value (ICOF-2, APS: 59.59 mol kg^{-1}) cannot compete with MOFs, of which the APS can be higher than 2000 mol kg^{-1}. We, therefore, concluded that MOFs perform better than COFs for adsorption-based separation of dry flue gas at VSA condition.

Calculated CO_2 selectivities of COFs at PSA and TSA conditions were between 1–66 and 1–105, respectively, whereas CO_2 working capacities were in the range of 0.18–6.36 mol kg^{-1} and 0.02–1.83 mol kg^{-1} as shown in Fig. 1(b) and (c), respectively. APSs of MOFs at PSA (TSA) condition were calculated to vary between 0.65 and 153.64 mol kg^{-1} (0.04 and 158.79 mol kg^{-1}). Although selectivities of COFs at PSA were computed to be lower than those calculated at VSA and TSA conditions, APSs of COFs were found to be the highest at PSA because of the high CO_2 working capacities. None of the COFs was able to surpass APS = 100 mol kg^{-1} curve at VSA condition while 5 COFs were identified to have APSs > 100 mol kg^{-1} at PSA condition as shown in Fig. 1(b), and only one COF exceeds APS = 100 mol kg^{-1} target at TSA condition as shown in Fig. 1(c). The COF that exceeds the APS target in TSA (ICOF-2) has Li$^+$ cations which significantly contributed to coulombic interactions between COF atoms and CO_2 molecules. Our simulation results showed that electrostatic interactions were responsible for 89% of the total interaction energy between this COF and guest molecules. Since the quadrupole moment of N_2 (4.65×10^{-40} C × m^2) is smaller than that of CO_2 (14.27×10^{-40} C × m^2),[65] electrostatic interactions become more pronounced for CO_2 than N_2.

Regenerability (R%) is an essential factor when assessing the practical usage of adsorbents for cyclic processes and it should be taken into account when selecting the most promising materials for cyclic VSA, PSA and TSA processes.[66] This is because adsorbents offering high selectivities generally suffer from low R% values. Calculated R% of COFs are shown as a function of their APSs in Fig. 2 where the red dashed line represents R% = 85 which we set as the minimum acceptable R%. High R% of COFs were generally obtained at VSA and PSA conditions as shown in Fig. 2(a) and (b), respectively, and COFs were found to have higher R% than most MOFs as shown in Fig. 2(a). More than 80% of COFs were computed to have R% >

85% at VSA and PSA conditions while this ratio was 18% at TSA condition. At VSA and PSA conditions R% values were generally high but tend to decrease as APS increases, which was previously observed for MOFs in adsorption-based CH_4/H_2 separation.[66] This indicates that many COFs with high APSs suffer from low R%. For example, ICOF-2 would be a promising material at all cyclic adsorption process conditions we studied in this work if we only focused on selectivity and APS. However, R% was calculated to be very low for this COF (23.12% for VSA, 45.98% for PSA and 61.60% for TSA), which makes it practically unusable under these operating conditions.

Fig. 2(c) shows that R% values computed for TSA condition were generally lower than the ones obtained at VSA and PSA conditions. Also, interestingly, these R% values showed a different trend than those computed for VSA and PSA conditions and increased as a function of APS. When we consider the calculation of APS ($S_{ads} \times \Delta N$), R% ($\Delta N/N_{ads}$), and ΔN ($N_{ads} - N_{des}$), only the amount of gas at the desorption condition (N_{des}) is different for VSA and TSA processes as both share the same adsorption temperature and pressure (1 bar, 298 K). Therefore, a higher R% at either of these conditions indicates that a higher amount of CO_2 is desorbed. At the desorption condition of TSA (1 bar, 393 K), adsorbed gas molecules did not desorb as much as at desorption condition of VSA (0.1 bar, 298 K) for most of the COFs, especially the ones with APS <10 mol kg^{-1}. This is shown in Fig. S3† where higher N_{des} indicates that less amount of gas is desorbed. Based on this, we can conclude that pressure have a more pronounced effect on gas desorption than temperature for most COFs.

We aimed to identify the most promising adsorbent candidates in each process by specifically focusing on COFs with R% > 85% and ranking them based on their APSs. COFs with R% > 85% were found to have APSs in the range of 0.07–58.95 mol kg^{-1} at VSA, 0.65–39.70 mol kg^{-1} at PSA and 0.74–63.43 mol kg^{-1} at TSA conditions. 10 COFs with the highest APSs were selected for each operating condition as the most promising materials and shown by red stars in Fig. 2. Among these, COF-42-gra, FLT-COF-1-staggered, COF-JLU3 and NPN-2 were the common top materials for VSA and TSA processes. Calculated adsorbent performance metrics and the names of the top COFs are given in Table 2 along with the selectivities and working capacities of some commercial adsorbents used in the industry to compare flue gas separation performances of different materials. Unit cell representations of the most promising COFs for each process condition are given in Fig. S4.† Table 2 shows that many of the promising COF adsorbents have higher CO_2/N_2 selectivities than commercial adsorbents while having comparable working capacities to them. For example, zeolite 13X provided a selectivity of 17 at 1 bar, 298 K and working capacity of 2.30 mol kg^{-1} at VSA conditions. The selectivities and working capacities of the top COFs of VSA condition were in the range of 14–40 and 0.58–1.67 mol kg^{-1}, respectively. This indicates that COFs have the potential to replace zeolites in adsorption-based CO_2/N_2 separation. The top COFs identified for TSA process have higher APSs compared to the top COFs identified for VSA and PSA conditions, suggesting that when APS and R% were both considered, TSA can be the best process
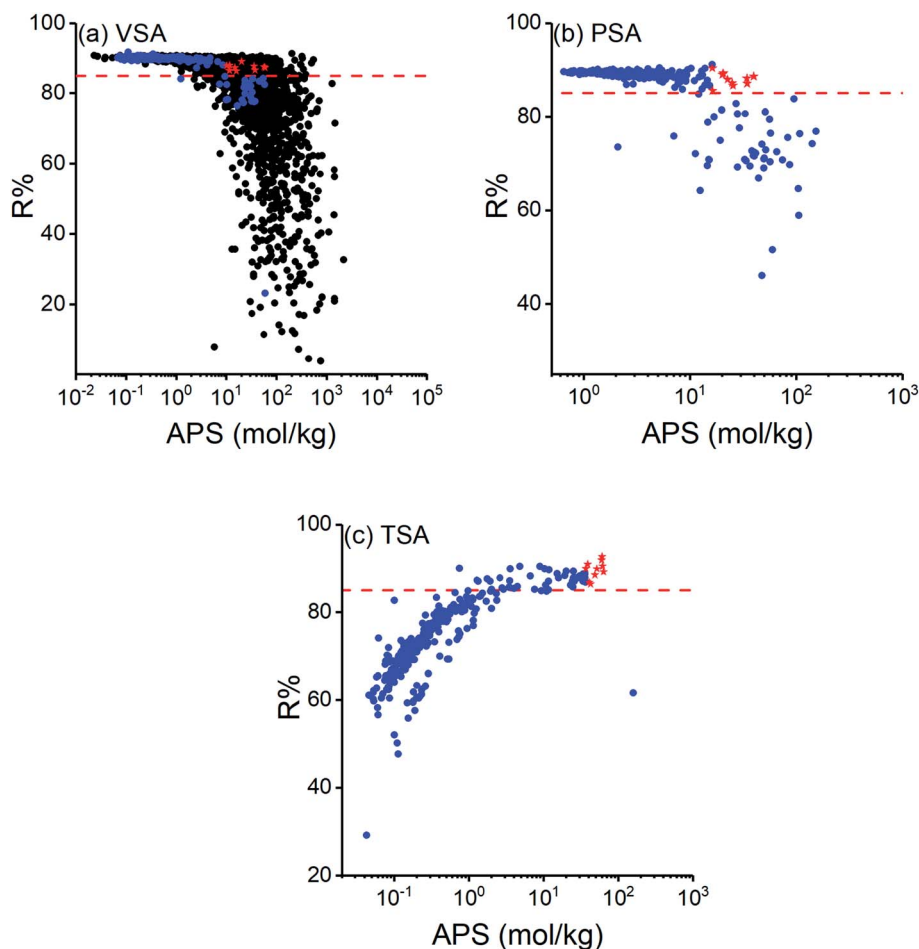
This journal is © The Royal Society of Chemistry 2020

J. Mater. Chem. A, 2020, **8**, 14609–14623 | **14613**

Fig. 2 Calculated $R\%$ and APS of COFs for CO_2/N_2 : 15/85 mixture under (a) VSA, (b) PSA, (c) TSA conditions. The red dotted line represents $R\% = 85\%$. Blue dots represent COFs while red stars represent the top 10 COFs identified at each condition. $R\%$ and APSs of MOFs (black dots) are also included for comparison in (a).

option for adsorption-based flue gas separation using COFs. Most COFs have high thermal stability[37] but to ensure if the top COFs that we identified for TSA process can be robust under temperature changes, we confirmed the thermal stabilities of these top COFs by checking their experimental synthesis papers. For instance, one of the promising COFs, 3D-COOH-COF, was reported to be thermally stable up to 723 K (ref. 67) and another promising COF, COF-42-gra, was thermally stable up to 553 K.[68] These temperatures are much higher than the desorption temperature of the TSA condition, 393 K, that we considered in this work.

After identifying the top COF adsorbents, we investigated the separation performances of these materials under humid conditions by performing GCMC simulations for ternary $CO_2/N_2/H_2O$ mixture. We first calculated the Henry's constants of water ($K_{H, water}$) for these COFs and found that $K_{H, water}$ values of 15 of the 26 distinct top COFs (top 10 COFs were identified for each process and 4 top materials were common for VSA and TSA) were smaller than that of ZIF-8 (6.21×10^{-6} mol kg^{-1} Pa^{-1}), which is known to be a hydrophobic MOF.[69,70] Therefore, it was seen that most of the top COFs we studied were also hydrophobic. Then, we performed adsorption simulations for

wet flue gas, *i.e.* $CO_2/N_2/H_2O$ mixture. Calculated CO_2 selectivities of hydrophobic COFs for wet flue gas were found to be only slightly lower (6–56 and 7–61 at 1 and 10 bar, respectively) than those computed for dry flue gas (7–77 and 7–66 at 1 and 10 bar, respectively). However, COFs having higher $K_{H, water}$ values were found to have significantly lower CO_2 selectivities for wet flue gas compared to those calculated for dry flue gas. For example, CO_2 selectivities of CuP-TFPh COF ($K_{H, water} = 3.12 \times 10^{-4}$ mol $kg^{-1} Pa^{-1}$) decreased from 17 to 1 at 1 bar and from 13 to 3 at 10 bar when ternary $CO_2/N_2/H_2O$ mixture was considered. We, therefore, concluded that humidity decreases the CO_2 selectivities of hydrophilic COFs in agreement with the results obtained when MOFs were studied for wet flue gas separation,[71] but hydrophobic COFs retained their high CO_2 selectivities in the presence of humidity.

3.2 Effects of structural curations on the simulated performances of COFs

We aimed to compare performances of COFs for CO_2/N_2 separation with those of MOFs. Therefore, COF structures in this work were taken from the CoRE COF database and used without

14614 | *J. Mater. Chem. A*, 2020, **8**, 14609–14623

This journal is © The Royal Society of Chemistry 2020

Table 2 Separation performances of the top 10 COFs computed at VSA, TSA, and PSA conditions and their comparison with some conventional adsorbents

Top COFs	S_{ads}	ΔN (mol kg^{-1})	APS (mol kg^{-1})	$R\%$
Vacuum swing adsorption (VSA)				
COF-42-gra	40.20	1.41	56.70	87.54
COF-43-gra	24.75	0.81	20.11	89.07
COF-JLU3	24.91	1.43	35.65	87.74
CuP-TFPh COF	16.78	0.94	15.71	86.35
FLT-COF-1 staggered	35.28	1.67	58.95	87.30
NPN-2	25.26	1.47	37.11	86.64
Ph-AnCD-COF	14.03	0.82	11.51	86.51
PyTTA-BFBIm-iCOF	16.96	0.88	14.87	87.33
TpMA	21.77	0.47	10.15	87.83
Tp-Por COF-AB	19.98	0.58	11.58	87.98
Pressure swing adsorption (PSA)				
COF-102	6.16	2.63	16.19	90.38
COF-300	9.52	2.65	25.28	86.63
COF-6	10.84	1.86	20.14	89.01
COF-DL229-6 fold	10.40	2.40	24.92	87.21
EB-COF:F	18.52	1.86	34.38	87.08
SIOC-COF-4-AB	7.17	2.27	16.29	85.53
TPE-COF-I	12.03	3.30	39.70	88.63
TPE-Ph COF	8.07	2.79	22.52	87.95
TpPa-1-F$_2$	12.83	1.60	20.52	89.28
TpPa-F$_4$	18.17	1.88	34.21	88.21
Temperature swing adsorption (TSA)				
3D-COOH-COF	76.52	0.78	59.58	91.89
COF-42-gra	40.20	1.49	60.05	92.70
COF-JLU3	24.91	1.47	36.55	89.97
CoPc-PorDBA^c	27.89	1.74	48.48	88.48
FLT-COF-1 staggered	35.28	1.73	61.11	90.51
NPN-1^b	30.45	1.68	51.27	89.90
NPN-2	25.26	1.54	38.95	90.94
PI-COF	34.71	1.83	63.43	89.23
POR-COF	26.09	1.39	36.18	86.82
TThPP	28.51	1.42	40.47	86.82

^{a} Calculated using Ideal adsorbed solution theory (IAST).[87] ^{b} This COF was reported to lose its crystal structure upon solvent removal.[88] ^{c} This COF was reported without Co atoms in databases.[89]

Adsorbents	Conventional adsorbents		
	S_{ads}	ΔN (mol kg^{-1})	Ref.
NaX	226.00 (IAST^a, 15 : 85, 298 K)	1.47 (1–0.1 bar)	81
NaY	14.84 (ideal, 1 bar, 303 K)	1.87 (1–0.1 bar)	82
Zeolite 13X	17.45 (ideal, 1 bar, 298 K)	2.30 (1–0.1 bar)	83
CHA	27.00 (ideal, 1 bar, 300 K)	3.60 (10–1 bar)	84
Hβ	11.33 (ideal, 1 bar, 300 K)	1.43 (1–0.1 bar)	85
Activated carbon	8.86 (ideal, 1 bar, 293 K)	2.58 (1–0.1 bar)	86

further optimization as we previously did in our large-scale screening of the MOF database.[10] While we were working on CoRE COFs, CURATED COF database, geometry optimized by considering symmetry and stacking of structures with a more detailed procedure than that of CoRE COFs,[40,43] was reported. The main input of our molecular simulations is the crystal structures of COFs. Therefore, we aimed to understand how

structural differences due to different optimization methods will affect simulation results and hence predicted flue gas separation performances of COFs. To investigate this, we focused on the top COFs identified from the CoRE COF database, computed their adsorbent performance metrics, and compared them with those computed for CURATED COFs. 9 (8) of the top COFs identified for PSA (VSA) process were available in CURATED COF database and all top performing COFs identified for TSA were available in the CURATED COF database.

We arranged the size of the data points in Fig. 3 according to the ratio of a structural property (ASA, ρ, and ϕ) of a CURATED COF to that of a CoRE COF and related the change in the calculated performance metrics to the change in the COF structure. The most significant change was observed for ASA of COFs. Fig. 3 shows the change in calculated APSs of COFs at VSA, PSA and TSA conditions according to ASA$_{CURATED}$/ASA$_{CoRE}$. The minimum, average, and maximum ratio of ASAs of CURATED and CoRE COFs (ASA$_{CURATED}$/ASA$_{CoRE}$) were calculated as 0.30, 0.69, and 1.16, respectively. If a COF is shown with a clearly different symbol size that means its ASA was significantly different when it was taken from CoRE COFs or CURATED COFs. APSs of COFs significantly changed especially when the structure optimization led to very different ASAs as presented with the symbol size in Fig. 3. It is important to note that the CURATED COFs do not only differ from CoRE COFs because of the detailed geometry optimization but they were also reported with high accuracy partial charges. In order to isolate the charge effect, we compared performance metrics under three different cases in Fig. 3: (i) when the coulombic interactions between adsorbents and gas molecules were neglected (blue points), (ii) when the charges of both COFs were assigned using the Q_{eq} method (black points), and (iii) when the charges of CoRE COFs were assigned using the Q_{eq} method while the charges of CURATED COFs were taken as the density-derived electrostatic and chemical charges-DDEC (red points). With case (i) and (ii) we examined only the effect of structural discrepancies on performance metrics while with case (iii) combined effect of different structural properties and different partial charges on performance metrics was investigated. Fig. 3(a) shows that APSs of most COFs significantly change for all three cases at VSA conditions. The coefficients of determination (R^2) between APSs of CoRE and CURATED COFs were calculated as 0.35 for case (i), 0.10 for case (ii) and 0.07 for case (iii) at VSA condition. In case (i), only the effect of geometry optimization was considered and the highest changes in APSs were observed for the COFs with the highest ASA$_{CURATED}$/ASA$_{CoRE}$ values. This can be explained with the change in the confinement and interaction of gas molecules with the COF's pores as these interactions are dominant at low pressures as in VSA process. The change in APSs of COFs taken from different databases was mainly due to working capacities rather than selectivities as shown in Fig. S5.† The difference in structural properties between the CURATED and CoRE version of a COF significantly affected the CO$_2$ uptakes (given in Fig. S6†), leading to considerably different working capacities. When we included the contribution of electrostatic interactions between COFs–guests in case (ii), larger changes were observed in APSs.
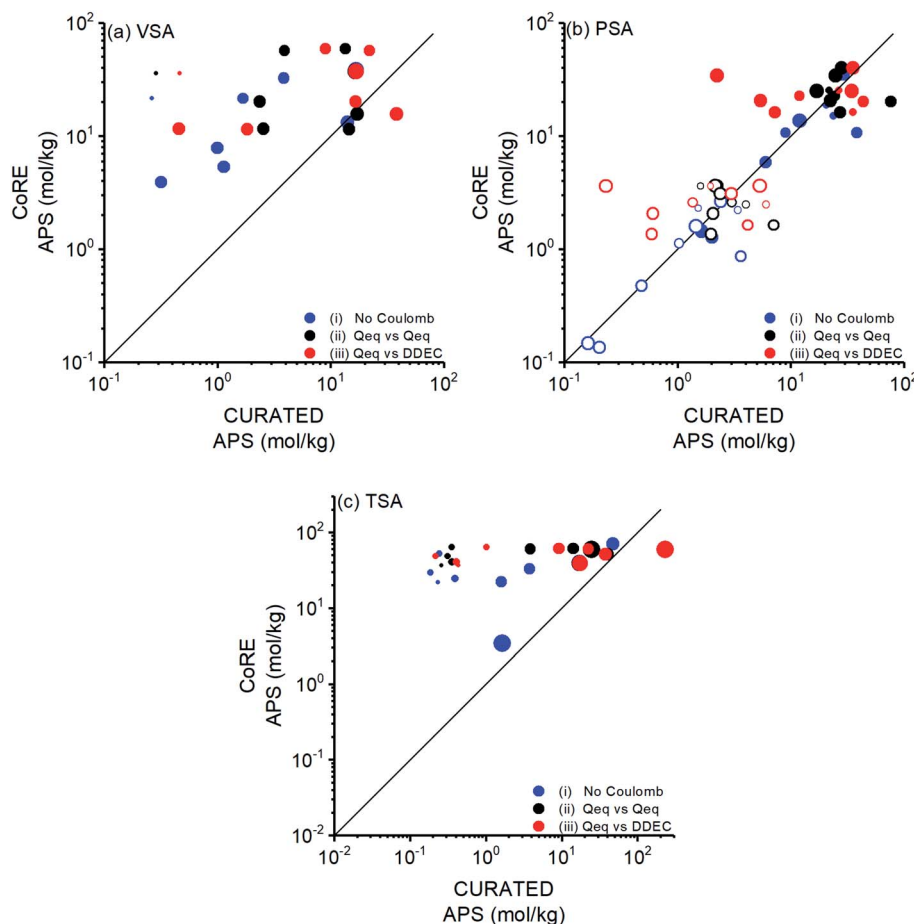
This journal is © The Royal Society of Chemistry 2020

J. Mater. Chem. A, 2020, **8**, 14609–14623 | **14615**

Fig. 3 Comparison of APSs of CURATED and CoRE COFs for (a) VSA, (b) PSA, and (c) TSA conditions. Symbols are sized based on ASA$_{CURATED}$/ASA$_{CoRE}$ while the regular size of the symbols can be seen in the legend. Hollow symbols in (b) represent calculated APSs of the top COFs identified for PSA process at VSA conditions.

The largest deviation in APS was observed in case (iii) due to the combined effect of structural discrepancy and different charges of CoRE COFs and CURATED COFs. In Fig. 3(a), the effect of different partial charges on APS values was clearly isolated for the COFs with ASA$_{CURATED}$/ASA$_{CoRE}$ value of ~1 (shown with standard symbol size). For one of these COFs, APS value decreased to half when the structure was taken from the CURATED database, showing the impact of using high accuracy charges on the performance predictions of COFs.

The top COFs selected for PSA process were found to have similar structures in CoRE and CURATED COF databases as shown by the size of the data points in Fig. 3(b). As a result, their predicted APSs were found to be strongly correlated for case (i) and (ii) leading to R^2 values of 0.85 and 0.69 (excluding the COF with the highest deviation), respectively. The stronger correlation at PSA compared to VSA condition can be due to the COF–guest interactions which are less significant at higher pressure of PSA. However, again higher deviations were observed in APSs for case (iii) (R^2 value of 0.27, excluding the same COF) due to the effect of DDEC charges on selectivity as shown in Fig. S7† with red points. We also computed APSs of the top COFs identified for PSA process at VSA conditions and showed them

with hollow symbols in Fig. 3(b). APSs of these COFs were found to be correlated leading to R^2 values of 0.78, 0.49, and 0.26 for case (i), (ii), and (iii), respectively. R^2 values of these COFs were not as low as the ones obtained for the top COFs of VSA process, indicating that structural properties have less effect on the performance of the top COFs of the PSA process. Finally, for TSA process, most of the top COFs had high deviations in their ASAs and APSs upon structural curation as shown in Fig. 3(c) similar to the top COFs of VSA process. The calculated R^2 values were 0.43 for case (i), 0.08 for case (ii), and 0.10 for case (iii). Both working capacity and selectivity changed when the curated structures were used in molecular simulations but the change in working capacity was more significant as shown in Fig. S8.†

It is not directly possible to apply detailed geometry optimization to a large number of COF structures and assign high accuracy partial charges. However, this comparison between databases suggested that predicted APSs of the top COFs whose structures were taken from CoRE COF database might be different from those taken from CURATED COF database, especially at low pressures where COF–gas interactions are important and more dependent on the structural properties. Sharma *et al.*[72] similarly showed that optimized slipped COF

14616 | *J. Mater. Chem. A*, 2020, **8**, 14609–14623

This journal is © The Royal Society of Chemistry 2020

structures have significantly different CO_2/N_2 selectivities than their counterparts. Therefore, detailed geometry optimization of COFs before simulations needs to be considered especially for VSA and TSA processes. We so far discussed the change in APS with respect to change in ASA, but change of APS with respect to changes in ρ and ϕ was also examined as shown in Fig. S9 and S10.† Overall, except for PSA, higher working capacities and higher selectivities were predicted when the structures were taken from CoRE database. As a result of this, higher APSs were obtained for CoRE COFs compared to CURATED COFs. Assigning partial charges to large numbers of COFs using approximate charge methods is computationally very efficient, however we suggest performing molecular simulations using CURATED COFs with high accuracy charges to make a final assessment about the potential of a COF adsorbent for VSA and TSA processes. We finally note that we only compared a small number of COFs from CoRE and CURATED databases and there is still much work needed to fully understand the dependence of simulated separation performance of COFs on the structures taken from different databases.

3.3 Membrane-based separation performance of COFs

We also examined membrane-based flue gas separation performances of 295 COFs. Adsorption, diffusion, and membrane selectivities of COFs computed at two different feed pressures, 1 and 10 bar, are shown in Fig. 4(a) and (b), respectively. Adsorption selectivities of all COFs were calculated to be greater than unity since CO_2 is more strongly adsorbed than N_2 as discussed in the previous section. Strong adsorption of CO_2 molecules resulted in their slow diffusion and diffusion selectivity mostly favored N_2. Diffusion of N_2 was significantly higher than that of CO_2 for 63 COFs at 1 bar and for 45 COFs at 10 bar as shown with black points in Fig. 4(a and b), respectively. In 23 (19) of these COFs at 1 bar (10 bar) CO_2 adsorption selectivities dominated high N_2 diffusion selectivity, leading to membranes with CO_2 selectivities >2. However, using these COFs as adsorbents can still be a better choice since they have higher adsorption selectivities than their membrane selectivities. In a single COF at 1 bar (Fig. 4(a)) and 4 COFs at 10 bar (Fig. 4(b)), CO_2 molecules diffuse faster than N_2 molecules, shown by blue dots, resulting in diffusion selectivities for CO_2 higher than
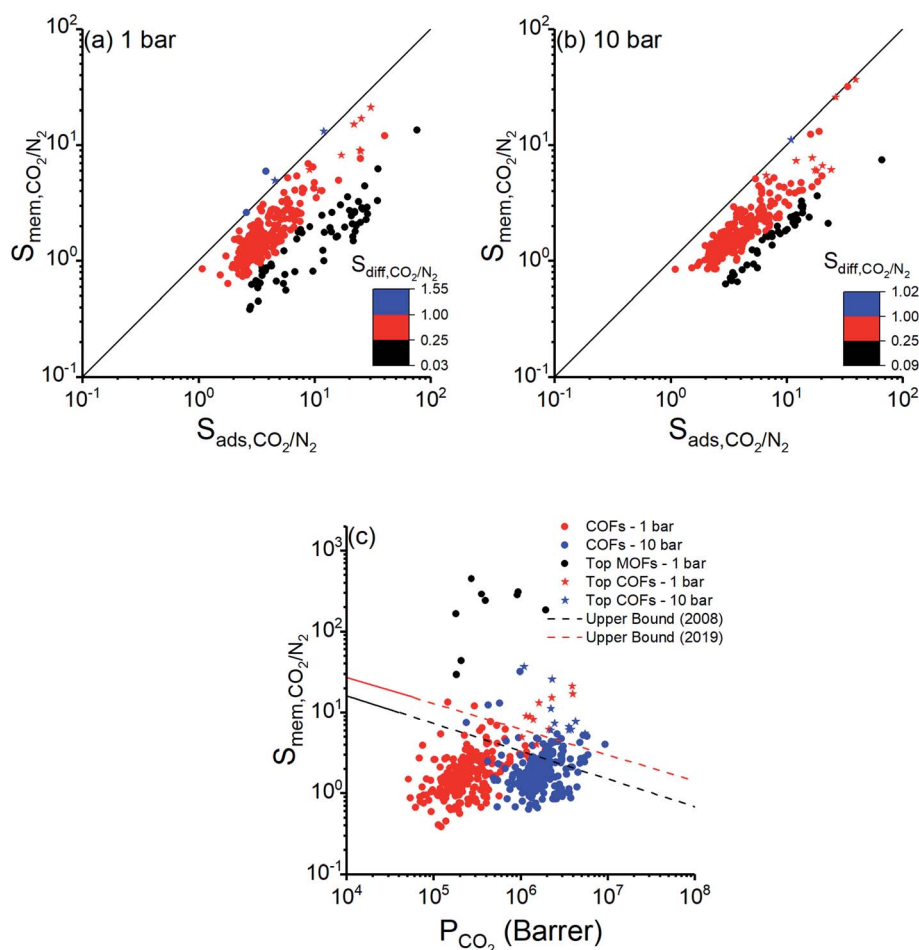

Fig. 4 Adsorption, diffusion, and membrane selectivities of COFs computed at (a) 1 bar, (b) 10 bar. Stars represent the top 10 COF membranes. (c) CO_2 permeability and membrane selectivity of COFs for separation of CO_2/N_2 : 15/85 mixture calculated at 1 and 10 bar presented together with upper bounds for polymeric membranes.[73,74] Separation performances of the top MOF membranes are also shown for comparison of COFs with MOFs.

This journal is © The Royal Society of Chemistry 2020

J. Mater. Chem. A, 2020, **8**, 14609–14623 | **14617**

unity. In these COFs, CO_2 was favored both by adsorption and diffusion. The best selectivities for COF membranes were achieved when adsorption strongly favored CO_2 and diffusion slightly favored N_2, as shown by red points in Fig. 4. Membrane selectivities of small number of materials, 49 COFs at 1 bar and 23 COFs at 10 bar, were calculated to be less than 1, indicating that these COF membranes are N_2 selective due to their high N_2 diffusion selectivity dominating their CO_2 adsorption selectivity. As a result of these, membrane selectivities of COFs were calculated to be between 0.38–21 and 0.63–37 at 1 bar and 10 bar, respectively.

Fig. 4(c) represents CO_2/N_2 membrane selectivities of COFs as a function of CO_2 permeabilities. CO_2 selectivities and permeabilities of the best performing MOF membranes identified in a previous work of our group[26] at 1 bar were also shown in Fig. 4(c). COF membranes offer similar permeabilities with the top MOF membranes, however selectivities of COF membranes were calculated to be lower, 0.38–21, than those of MOFs, 29–449. This can be explained by the large pore sizes and/or lack of metal sites in COFs as we discussed above. Robeson's upper bound,[73] which is the upper limit for the separation performance of polymer membranes, and the new upper bound,[74] which was recently updated considering CO_2/N_2 separation performances of ultrapermeable polymers of intrinsic microporosity, are also shown in Fig. 4(c). Due to their low selectivities, only a small number of COFs exceeded the upper bounds. On the other hand, we extended these upper bounds because COFs have very high CO_2 permeabilities, ranging from 5.12×10^4 to 3.96×10^6 barrer at 1 bar and from 2.39×10^5 to 9.30×10^6 barrer at 10 bar. The most promising COF membranes offering CO_2 permeabilities $>10^6$ barrer and the highest selectivities are shown by stars in Fig. 4(c) and

detailed information about their calculated membrane metrics are given in Table 3.

3.4 Structure–performance analyses of COFs

Finally, we investigated structure–performance relations of COFs to estimate the best combination of structural properties leading to a good CO_2/N_2 separation performance of a COF. Fig. 5(a and b) shows the relation between CO_2/N_2 selectivity of COF adsorbents calculated at 1 bar and 10 bar, porosity and LCD of 295 COFs. Selectivities of COFs increase as LCD and porosity decrease due to the better confinement of gas molecules inside the narrow pores.[75] However, some COFs with LCD > 9 Å and $\phi > 0.6$ did not follow the same trend, and their CO_2/N_2 selectivities were relatively high although they had large pores. To further investigate this, we performed GCMC simulations for these COFs by switching-off the coulombic interactions between COFs and adsorbate molecules. The triangles in Fig. 5(a and b) show selectivities of these COFs which were calculated by neglecting the coulombic interactions in molecular simulations. Selectivities significantly decreased when the electrostatic interactions were neglected and we changed the color of the symbols in Fig. 5(a and b) according to the coloring scale used for selectivity when all the interactions were considered in molecular simulations. The most remarkable difference was observed for the selectivity of ICOF-2, which decreased from 105 to 4, when the coulombic interactions between this COF and CO_2 molecules were neglected. Electrostatic interactions between the host and adsorbates significantly contributed to the total energy of this COF, as discussed before, due to the existence of B and Li ions with large partial charges ($1.28e^-$ for B ions and $1.12e^-$ for Li ions). Therefore, we concluded that COFs with large pores generally suffer from low adsorption selectivity

Table 3 Performances of the top 10 COFs for membrane-based CO_2/N_2 separation

Top COFs	D_{self,CO_2} (10^{-5} cm^2 s^{-1})	D_{self,N_2} (10^{-4} cm^2 s^{-1})	P_{CO_2} (10^6 barrer)	P_{N_2} (10^5 barrer)	$S_{ads,CO_2/N_2}$	$S_{diff,CO_2/N_2}$	$S_{mem,CO_2/N_2}$
1 bar							
CC-TAPH-COF	7.27	1.97	1.16	1.27	24.51	0.37	9.03
COF-JLU3	8.88	2.49	1.27	1.43	24.91	0.36	8.87
CTF-FUM	28.50	4.18	2.12	3.48	9.02	0.68	6.15
MPCOF	55.20	5.08	1.03	2.11	4.55	1.09	4.94
NPN-1	9.98	1.44	3.91	1.83	30.45	0.69	21.13
NPN-2	12.00	1.78	3.96	2.32	25.26	0.67	16.98
NPN-3	12.33	1.12	1.61	1.24	12.00	1.10	13.18
PyTTA-BFBIm-iCOF	8.01	1.66	1.39	1.69	16.96	0.48	8.18
TEMPO-COF	33.24	9.02	1.51	3.77	10.90	0.37	4.02
TpMA	17.16	2.46	2.27	1.50	21.77	0.70	15.19
10 bar							
CC-TAPH-COF	6.58	1.40	4.28	5.52	16.58	0.47	7.78
COF-JLU3	5.90	1.80	3.58	5.39	20.31	0.33	6.66
CTF-1	26.44	3.20	5.46	9.90	6.64	0.83	5.49
CTF-FUM	6.33	6.20	2.22	2.00	10.91	1.02	11.14
FLT-COF-1 staggered	4.82	1.90	3.81	6.21	24.16	0.25	6.14
NPN-1	1.15	1.23	1.09	0.30	39.39	0.93	36.56
PyTTA-BFBIm-iCOF	4.81	1.38	3.56	5.85	17.49	0.35	6.09
TPE-COF-I	4.34	7.11	2.46	3.35	12.03	0.61	7.34
TpMA	5.08	5.23	2.29	0.89	26.48	0.97	25.76
TpPa-F$_4$	5.13	1.55	2.22	3.71	18.17	0.33	6.02

14618 | *J. Mater. Chem. A*, 2020, **8**, 14609–14623

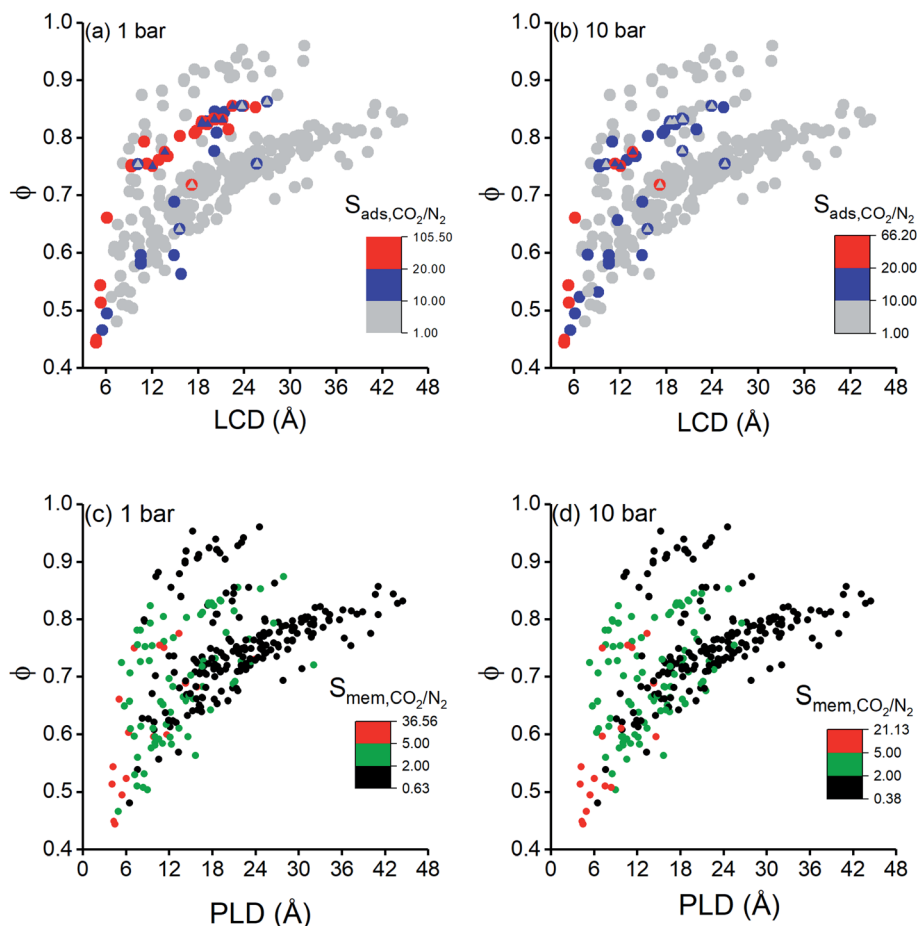This journal is © The Royal Society of Chemistry 2020

Fig. 5 LCDs and porosities of COFs as a function of their adsorption selectivities calculated at (a) 1 bar, (b) 10 bar. COFs are colored according to their adsorption selectivities in (a) and (b). Triangles represent calculated selectivities of COFs when the coulombic interactions were neglected. PLDs and porosities of COFs as a function of their membrane selectivities calculated at (c) 1 bar and (d) 10 bar, respectively. Colors represent membrane selectivity of COFs in (c) and (d).

but the ones having metal atoms with relatively large partial charges could offer high selectivities even if they are large-pored. Fig. 5(a) has a wider distribution of CO_2/N_2 selectivities and more outliers than Fig. 5(b) because the coulombic interactions between the adsorbent and adsorbates become more pronounced at low pressures. Similar to adsorption selectivity-LCD relation, we also studied membrane selectivity-PLD correlation. Fig. 5(c and d) shows the relation between CO_2/N_2 selectivity of COF membranes calculated at 1 bar and 10 bar, porosity and PLD of 295 COFs. Membrane selectivities of COFs decrease as their PLDs and porosities increase because both gases can easily diffuse through the large pores, limiting the separation capacity of membranes. Results in Fig. 5(a–d) showed that pore size has a greater importance than porosity on the CO_2 selectivity of COFs since for a specific porosity a wide variety of selectivity values could be obtained according to the pore sizes of the COFs.

We finally aim to elucidate the optimum structural properties of COFs to achieve high CO_2/N_2 separation performances and to compare these optimum structural properties with those of MOFs. Fig. 6 shows computed structural properties of all

COFs that we studied in this work, the top 10 promising COF adsorbents identified for each cyclic adsorption process, VSA, PSA, and TSA, and the top 10 promising COF membranes. For both adsorption- and membrane-based flue gas separation, COFs with pore sizes (PLD and LCD) <10 Å offer the best performances. For adsorption-based separation, COFs with 2000 m^2 g^{-1} < ASA <4500 m^2 g^{-1} and 0.6 < ϕ <0.8 were identified to achieve the highest APS values whereas for membrane-based separation, COFs with ASA <2000 m^2 g^{-1} and ϕ < 0.6 were identified to have the highest selectivities. Previously, it was shown that MOFs with pore sizes <7.5 Å, ASA <1000 m^2 g^{-1}, and 0.5 < ϕ < 0.75 can have high CO_2/N_2 adsorption and membrane selectivities.[10,26] Promising COF adsorbents and COF membranes have slightly larger pore sizes, similar porosities, and higher surface areas compared to promising MOFs for CO_2/N_2 separation. We finally note that chemical properties of COFs, e.g. type of framework atoms, presence of metal atoms and functional groups in the frameworks, also effect CO_2 adsorption, but we solely focused on the effects of structural properties, such as pore size and surface area which are easily calculated with computational methods, on the predicted
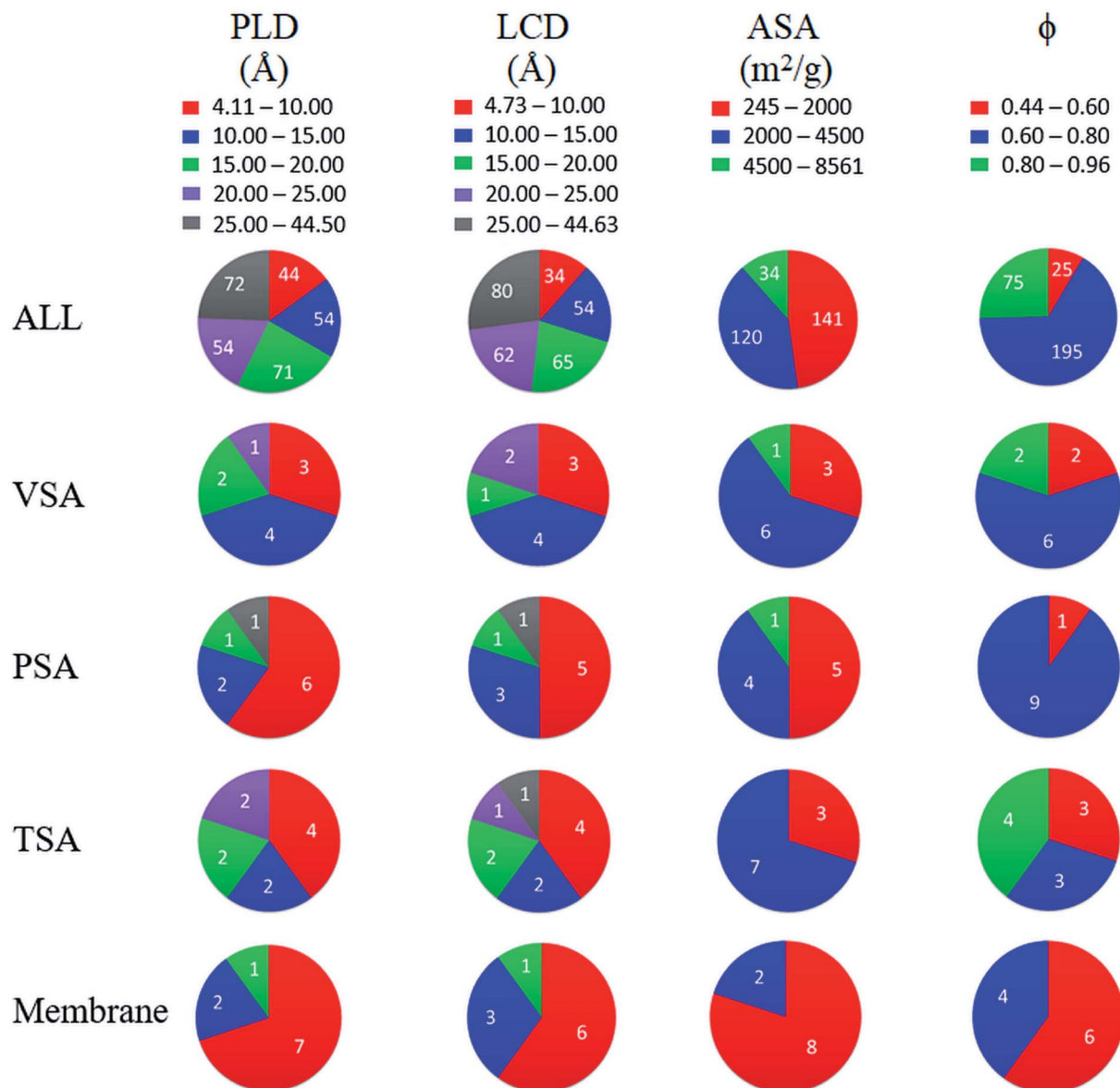
This journal is © The Royal Society of Chemistry 2020

J. Mater. Chem. A, 2020, **8**, 14609–14623 | **14619**

Fig. 6 Distribution of calculated PLD, LCD, ASA and ϕ of all 295 COFs and the top 10 COFs identified for each separation process. Numbers in the charts show the number of COFs.

separation performances of COFs in this work. These structure–performance relations will provide valuable information to experimentalists for the design and advancement of unique COF structures which realize highly selective CO_2/N_2 separations.

4. Conclusion

In this work CO_2/N_2 mixture separation potentials of 295 COFs were examined both for adsorption- and membrane-based applications by combining GCMC and MD simulations. Results of molecular simulations were utilized for predicting adsorption selectivity, working capacity, $R\%$, APS of COFs for three distinct cyclic adsorption processes, VSA, PSA, and TSA. Comparison of COFs with MOFs at VSA condition revealed that

COFs have lower selectivities (1–105) than MOFs (2–6107) due to their larger pores and the lack of metal sites in their frameworks. On the other hand, COFs offer working capacities between 0.02–1.69 mol kg^{-1} while this range was 0.01–4.16 mol kg^{-1} for MOFs at VSA conditions. Results also showed that COFs can have higher selectivities than currently used adsorbents, such as zeolites and activated carbons, while having similar working capacities to them. Therefore, COFs have the potential to replace conventional adsorbents for CO_2 separation from flue gas. For CO_2/N_2 separation using COFs as adsorbents, TSA process was suggested because more COFs were identified to have a combination of high $R\%$ (>85%) and high APS (>10 mol kg^{-1}) compared to VSA and PSA conditions. Molecular simulations also showed that selectivity of COFs do not significantly change in the presence of humidity, making them

14620 | *J. Mater. Chem. A*, 2020, **8**, 14609–14623

This journal is © The Royal Society of Chemistry 2020

potential adsorbents for wet flue gas separation. Curated, optimized COFs with high accuracy partial charges were computed to have lower APSs than CoRE COFs having approximate charges, especially if the structure was significantly affected from the geometry optimization. This showed the importance of using the correct COF structure before assessing its potential for CO_2/N_2 separation. Gas permeabilities of COF membranes (5.12×10^4 to 3.96×10^6 barrer) were computed to be similar to those of MOF membranes, however COFs suffered from low membrane selectivities (0.38–21). Due to their low selectivities, most COF membranes could not exceed the Robeson's upper bound.

These results answered the question raised in the title of our work: COFs have the potential to compete with MOFs in adsorption-based flue gas separations but their potential as CO_2 selective membranes is limited. However, several strategies such as functionalizing COFs by incorporating ionic liquids into COFs,[76,77] assisting COFs with graphene oxides to fabricate ultrathin membranes,[78] and using COFs as fillers in polymers to make mixed matrix membranes similar to MOFs[26,79,80] can enhance membrane selectivities of COFs by tuning their pore sizes and/or chemical properties. Results of structure–performance analysis that we provided in this work can be used to advance the design and development of new COF adsorbents and membranes with desired structural properties. We note that COF structures that we studied in this work have been already experimentally synthesized and reported in the computation-ready COF database. Large-scale production of MOFs has already started so we expect to see scalable production and industrial applications of COFs especially in gas storage and separation fields in near future. Finally, high-throughput computational screening of COFs that we used in this work can be applied to unlock the potential of COFs to separate various gas mixtures in future studies.

Conflicts of interest

There are no conflicts to declare.

Acknowledgements

References

1 T. Boden, R. Andres and G. Marland, *Global, regional, and national fossil-fuel CO₂ emissions (1751-2014)(v. 2017)*, Environmental System Science Data Infrastructure for a Virtual Ecosystem, 2017.

2 M. Songolzadeh, M. Soleimani, M. Takht Ravanchi and R. Songolzadeh, *Sci. World J.*, 2014, **2014**, 1–35.

3 D. Bahamon and L. F. Vega, *Chem. Eng. J.*, 2016, **284**, 438–447.

4 N. Hedin, L. Andersson, L. Bergström and J. Yan, *Appl. Energy*, 2013, **104**, 418–433.

5 R. Kumar, *Ind. Eng. Chem. Res.*, 1994, **33**, 1600–1605.

6 Y. S. Bae and R. Q. Snurr, *Angew. Chem., Int. Ed.*, 2011, **50**, 11586–11596.

7 D. M. D'Alessandro, B. Smit and J. R. Long, *Angew. Chem., Int. Ed.*, 2010, **49**, 6058–6082.

8 J. Jiang, *Mol. Simul.*, 2014, **40**, 516–536.

9 H. Deng, S. Grunder, K. E. Cordova, C. Valente, H. Furukawa, M. Hmadeh, F. Gándara, A. C. Whalley, Z. Liu, S. Asahina, H. Kazumori, M. O'Keeffe, O. Terasaki, J. F. Stoddart and O. M. Yaghi, *Science*, 2012, **336**, 1018–1023.

10 C. Altintas, G. Avci, H. Daglar, A. Nemati Vesali Azar, S. Velioglu, I. Erucar and S. Keskin, *ACS Appl. Mater. Interfaces*, 2018, **10**, 17257–17268.

11 S. Keskin, *Nat. Energy*, 2019, **5**, 8–9.

12 H. Furukawa, K. E. Cordova, M. O'Keeffe and O. M. Yaghi, *Science*, 2013, **341**, 974–988.

13 B. Liu and B. Smit, *Langmuir*, 2009, **25**, 5918–5926.

14 B. Liu and B. Smit, *J. Phys. Chem. C*, 2010, **114**, 8515–8522.

15 R. Krishna and J. M. J. S. van Baten, *Sep. Purif. Technol.*, 2012, **87**, 120–126.

16 Z. J. Zhang, Z. Z. Yao, S. C. Xiang and B. L. Chen, *Energy Environ. Sci.*, 2014, **7**, 2868–2899.

17 Q. Wang, J. Bai, Z. Lu, Y. Pan and X. You, *Chem. Commun.*, 2016, **52**, 443–452.

18 R. Ben-Mansour, M. A. Habib, O. E. Bamidele, M. Basha, N. A. A. Qasem, A. Peedikakkal, T. Laoui and M. Ali, *Appl. Energy*, 2016, **161**, 225–255.

19 E. Haldoupis, S. Nair and D. S. Sholl, *J. Am. Chem. Soc.*, 2012, **134**, 4313–4323.

20 D. Wu, Q. Yang, C. Zhong, D. Liu, H. Huang, W. Zhang and G. Maurin, *Langmuir*, 2012, **28**, 12094–12099.

21 C. E. Wilmer, O. K. Farha, Y. S. Bae, J. T. Hupp and R. Q. Snurr, *Energy Environ. Sci.*, 2012, **5**, 9849–9856.

22 Z. W. Qiao, K. Zhang and J. W. Jiang, *J. Mater. Chem. A*, 2016, **4**, 2105–2114.

23 Y. G. Chung, J. Camp, M. Haranczyk, B. J. Sikora, W. Bury, V. Krungleviciute, T. Yildirim, O. K. Farha, D. S. Sholl and R. Q. Snurr, *Chem. Mater.*, 2014, **26**, 6185–6192.

24 R. Krishna and J. M. van Baten, *Phys. Chem. Chem. Phys.*, 2011, **13**, 10593–10616.

25 T. Watanabe and D. S. Sholl, *Langmuir*, 2012, **28**, 14114–14128.

26 H. Daglar and S. Keskin, *J. Phys. Chem. C*, 2018, **122**, 17347–17357.

27 J. Liu, J. Tian, P. K. Thallapally and B. P. McGrail, *J. Phys. Chem. C*, 2012, **116**, 9575–9581.

28 A. C. Kizzie, A. G. Wong-Foy and A. J. Matzger, *Langmuir*, 2011, **27**, 6368–6373.

29 S. J. Datta, C. Khumnoon, Z. H. Lee, W. K. Moon, S. Docao, T. H. Nguyen, I. C. Hwang, D. Moon, P. Oleynikov, O. Terasaki and K. B. Yoon, *Science*, 2015, **350**, 302–306.

30 Y. Zeng, R. Zou and Y. Zhao, *Adv. Mater.*, 2016, **28**, 2855–2873.

This journal is © The Royal Society of Chemistry 2020

J. Mater. Chem. A, 2020, **8**, 14609–14623 | **14621**

31 O. Shekhah, Y. Belmabkhout, Z. Chen, V. Guillerm, A. Cairns, K. Adil and M. Eddaoudi, *Nat. Commun.*, 2014, **5**, 4228–4235.

32 P. Nugent, Y. Belmabkhout, S. D. Burd, A. J. Cairns, R. Luebke, K. Forrest, T. Pham, S. Ma, B. Space, L. Wojtas, M. Eddaoudi and M. J. Zaworotko, *Nature*, 2013, **495**, 80–84.

33 P. J. Waller, F. Gandara and O. M. Yaghi, *Acc. Chem. Res.*, 2015, **48**, 3053–3063.

34 A. P. Cote, A. I. Benin, N. W. Ockwig, M. O'Keeffe, A. J. Matzger and O. M. Yaghi, *Science*, 2005, **310**, 1166–1170.

35 C. S. Diercks and O. M. Yaghi, *Science*, 2017, **355**, 923–933.

36 U. Díaz and A. Corma, *Coord. Chem. Rev.*, 2016, **311**, 85–124.

37 X. Feng, X. Ding and D. Jiang, *Chem. Soc. Rev.*, 2012, **41**, 6010–6022.

38 H. M. El-Kaderi, J. R. Hunt, J. L. Mendoza-Cortes, A. P. Cote, R. E. Taylor, M. O'Keeffe and O. M. Yaghi, *Science*, 2007, **316**, 268–272.

39 M. Tong, Q. Yang and C. Zhong, *Microporous Mesoporous Mater.*, 2015, **210**, 142–148.

40 M. M. Tong, Y. S. Lan, Q. Y. Yang and C. L. Zhong, *Chem. Eng. Sci.*, 2017, **168**, 456–464.

41 M. M. Tong, Y. S. Lan, Z. L. Qin and C. L. Zhong, *J. Phys. Chem. C*, 2018, **122**, 13009–13016.

42 T. Yan, Y. Lan, M. Tong and C. Zhong, *ACS Sustainable Chem. Eng.*, 2018, **7**, 1220–1227.

43 D. Ongari, A. V. Yakutovich, L. Talirz and B. Smit, *ACS Cent. Sci.*, 2019, **5**, 1663–1675.

44 K. S. Deeg, D. D. Borges, D. Ongari, N. Rampal, L. Talirz, A. V. Yakutovich, J. M. Huck and B. Smit, *ACS Appl. Mater. Interfaces*, 2020, **12**, 21559–21568.

45 T. F. Willems, C. H. Rycroft, M. Kazi, J. C. Meza and M. Haranczyk, *Microporous Mesoporous Mater.*, 2012, **149**, 134–141.

46 S.-Q. Xu, R.-R. Liang, T.-G. Zhan, Q.-Y. Qi and X. Zhao, *Chem. Commun.*, 2017, **53**, 2431–2434.

47 Z. Sumer and S. Keskin, *Ind. Eng. Chem. Res.*, 2016, **55**, 10404–10419.

48 D. Dubbeldam, S. Calero, D. E. Ellis and R. Q. Snurr, *Mol. Simul.*, 2016, **42**, 81–101.

49 R. Ben-Mansour and N. A. Qasem, *Energy Convers. Manage.*, 2018, **156**, 10–24.

50 C. E. Wilmer and R. Q. Snurr, *Chem. Eng. J.*, 2011, **171**, 775–781.

51 R. L. Akkermans, N. A. Spenley and S. H. Robertson, *Mol. Simul.*, 2013, **39**, 1153–1164.

52 P. P. Ewald, *Ann. Phys.*, 1921, **369**, 253–287.

53 B. L. Eggimann, A. J. Sunnarborg, H. D. Stern, A. P. Bliss and J. I. Siepmann, *Mol. Simul.*, 2014, **40**, 101–105.

54 J. J. Potoff and J. I. Siepmann, *AlChE J*, 2001, **47**, 1676–1682.

55 C. Murthy, K. Singer, M. Klein and I. McDonald, *Mol. Phys.*, 1980, **41**, 1387–1399.

56 S. L. Mayo, B. D. Olafson and W. A. Goddard, *J. Phys. Chem.*, 1990, **94**, 8897–8909.

57 C. Vega, J. Abascal and I. Nezbeda, *J. Chem. Phys.*, 2006, **125**, 34503–34513.

58 J. L. Abascal and C. Vega, *J. Chem. Phys.*, 2005, **123**, 234505–234517.

59 B. Widom, *J. Chem. Phys.*, 1963, **39**, 2808–2812.

60 D. Frenkel and B. Smit, *Understanding molecular simulation: From algorithms to applications*, Elsevier (formerly published by Academic Press), 2002.

61 A. Einstein, *Investigations on the theory of the Brownian movement*, Courier Corporation, 1956.

62 S. Keskin and D. Sholl, *Ind. Eng. Chem. Res.*, 2009, **48**, 914–922.

63 I. Erucar and S. Keskin, *J. Membr. Sci.*, 2016, **514**, 313–321.

64 R. Poloni, K. Lee, R. F. Berger, B. Smit and J. B. Neaton, *J. Phys. Chem. Lett.*, 2014, **5**, 861–865.

65 C. Graham, D. A. Imrie and R. E. Raab, *Mol. Phys.*, 1998, **93**, 49–56.

66 Y. Basdogan, K. B. Sezginel and S. Keskin, *Ind. Eng. Chem. Res.*, 2015, **54**, 8479–8491.

67 Q. Lu, Y. Ma, H. Li, X. Guan, Y. Yusran, M. Xue, Q. Fang, Y. Yan, S. Qiu and V. Valtchev, *Angew. Chem., Int. Ed.*, 2018, **57**, 6042–6048.

68 F. J. Uribe-Romo, C. J. Doonan, H. Furukawa, K. Oisaki and O. M. Yaghi, *J. Am. Chem. Soc.*, 2011, **133**, 11478–11481.

69 P. Z. Moghadam, D. Fairen-Jimenez and R. Q. Snurr, *J. Mater. Chem. A*, 2016, **4**, 529–536.

70 H. Zhang and R. Q. Snurr, *J. Phys. Chem. C*, 2017, **121**, 24000–24010.

71 I. Erucar and S. Keskin, *Ind. Eng. Chem. Res.*, 2020, **59**, 3141–3152.

72 A. Sharma, A. Malani, N. V. Medhekar and R. Babarao, *CrystEngComm*, 2017, **19**, 6950–6963.

73 L. M. Robeson, *J. Membr. Sci.*, 2008, **320**, 390–400.

74 B. Comesaña-Gándara, J. Chen, C. G. Bezzu, M. Carta, I. Rose, M.-C. Ferrari, E. Esposito, A. Fuoco, J. C. Jansen and N. B. McKeown, *Energy Environ. Sci.*, 2019, **12**, 2733–2740.

75 G. Avci, S. Velioglu and S. Keskin, *ACS Appl. Mater. Interfaces*, 2018, **10**, 33693–33706.

76 M. Zeeshan, V. Nozari, M. B. Yagci, T. Isık, U. Unal, V. Ortalan, S. Keskin and A. Uzun, *J. Am. Chem. Soc.*, 2018, **140**, 10113–10116.

77 L.-G. Ding, B.-J. Yao, F. Li, S.-C. Shi, N. Huang, H.-B. Yin, Q. Guan and Y.-B. Dong, *J. Mater. Chem. A*, 2019, **7**, 4689–4698.

78 Y. Ying, D. Liu, J. Ma, M. Tong, W. Zhang, H. Huang, Q. Yang and C. Zhong, *J. Mater. Chem. A*, 2016, **4**, 13444–13449.

79 X. Guo, Z. Qiao, D. Liu and C. Zhong, *J. Mater. Chem. A*, 2019, **7**, 24738–24759.

80 Y. Cheng, L. Zhai, Y. Ying, Y. Wang, G. Liu, J. Dong, D. Z. L. Ng, S. A. Khan and D. Zhao, *J. Mater. Chem. A*, 2019, **7**, 4549–4560.

81 M. Xu, S. Chen, D.-K. Seo and S. Deng, *Chem. Eng. J.*, 2019, **371**, 693–705.

82 P. J. Harlick and F. H. Tezel, *Microporous Mesoporous Mater.*, 2004, **76**, 71–79.

83 S. Cavenati, C. A. Grande and A. E. Rodrigues, *J. Chem. Eng. Data*, 2004, **49**, 1095–1101.

84 E. García-Pérez, J. Parra, C. Ania, A. García-Sánchez, J. Van Baten, R. Krishna, D. Dubbeldam and S. Calero, *Adsorption*, 2007, **13**, 469–476.

14622 | *J. Mater. Chem. A*, 2020, **8**, 14609–14623

This journal is © The Royal Society of Chemistry 2020

85 X. Xu, X. Zhao, L. Sun and X. Liu, *J. Nat. Gas Chem.*, 2008, **17**, 391–396.

86 X. Dong, J. Zhang, L. Gang, P. Xiao, P. Webley and Y.-c. Zhai, *J. Fuel Chem. Technol.*, 2011, **39**, 169–174.

87 A. L. Myers and J. M. Prausnitz, *AlChE J*, 1965, **11**, 121–127.

88 D. Beaudoin, T. Maris and J. D. Wuest, *Nat. Chem.*, 2013, **5**, 830–834.

89 V. S. P. K. Neti, X. Wu, M. Hosseini, R. A. Bernal, S. Deng and L. Echegoyen, *CrystEngComm*, 2013, **15**, 7157–7160.

This journal is © The Royal Society of Chemistry 2020

J. Mater. Chem. A, 2020, **8**, 14609–14623 | **14623**